

## Electronic Supplementary Information

### Critical Effect of Bottom Oxide Electrode on Ferroelectricity of Epitaxial $\text{Hf}_{0.5}\text{Zr}_{0.5}\text{O}_2$

#### Thin Films

Saúl Estandía,<sup>1</sup> Jaume Gàzquez,<sup>1</sup> María Varela,<sup>2</sup> Nico Dix,<sup>1</sup> Mengdi Qian,<sup>1</sup> Raúl Solanas,<sup>1</sup> Ignasi Fina,<sup>1</sup> and Florencio Sánchez<sup>1,\*</sup>

<sup>1</sup> Institut de Ciència de Materials de Barcelona (ICMAB-CSIC), Campus UAB, Bellaterra 08193, Spain

<sup>2</sup> Dpto. Física de Materiales & Instituto Pluridisciplinar, Universidad Complutense de Madrid, 28040, Madrid, Spain

\* fsanchez@icmab.es

#### S1 Definition of the XRD measuring angles

Figure S1 shows a sketch of the angles between the X-Ray incident and scattered beams and the sample. The  $\chi$  and  $\omega$  axes lay on the sample's surface, with  $\chi$  being also contained within the diffraction plane (plane containing the incident and scattered beams) and  $\omega$  being perpendicular to it.

The 2D detector of GADDS allows the simultaneous acquisition of diffracting planes parallel to the sample surface ( $\chi=0$ ) and tilted around the  $\chi$  axis ( $\chi \neq 0$ ) away from the sample's normal plane.

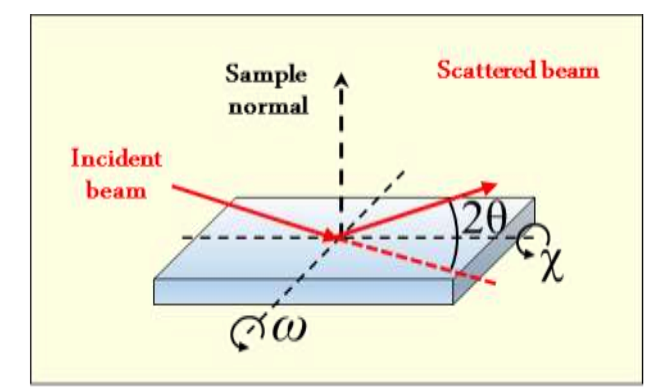


Figure S1. Sketch showing  $\chi$ ,  $\omega$  and  $2\theta$  angles. The solid red lines mark the trajectory of incident and scattered beams, while the dashed red line marks the trajectory of the unscattered beam inside the sample.

## S2 Zoomed I-V curves and polarization loops of HZO films on BLSO, SRO, Nb:STO, and LNO electrodes

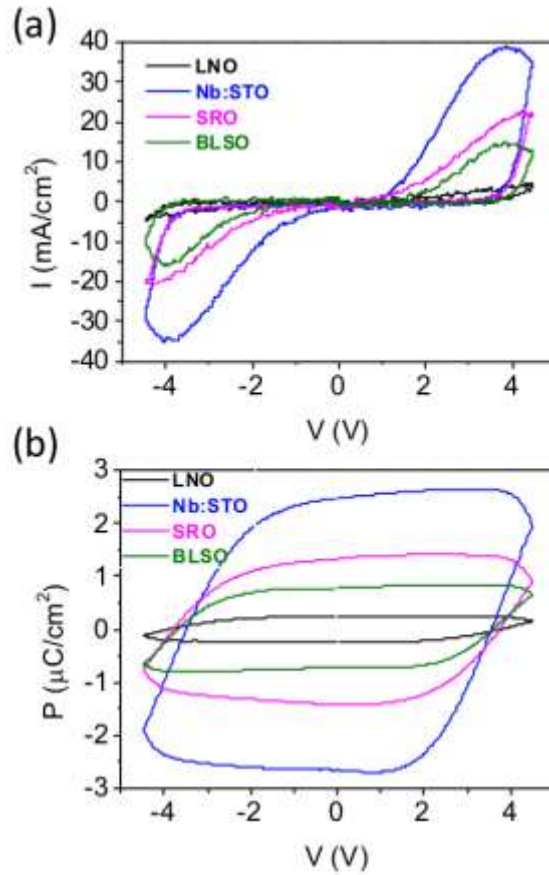


Figure S2. (a) I-V curves of the HZO films grown on STO buffered with LNO, SRO or BLSO and the HZO film grown on the Nb:STO crystal. (b) Corresponding polarization loops.

## S3 P-E loops collected during the first 10 cycles for HZO films on BLSO, SRO, Nb:STO, LSMO electrodes

In Figure S3, representative loops collected during the first 10 cycles in films grown on LSMO, SRO, Nb:STO and BLSO are shown. As reported,<sup>1</sup> epitaxial films can show a small wake-up effect. In Figure S3(a), this small effect is observed by the different shape of the pristine and second cycled loop compared with the tenth. More prominent is the change upon cycling observed in the HZO film grown on NSTO (Figure S3(b)) and BLSO (Figure 3(c)). Whereas, the first loop (in blue) shows a round shape, the successive cycling produces a reduction of integrated polarization and the loop gradually becomes more square-like. These results suggest that the pristine loop is dominated by residual leakage probably resulting from defects, which redistribute during the first cycles. The loops obtained for the HZO film on SRO also show an important change, although these do not show a saturated shape in any case.

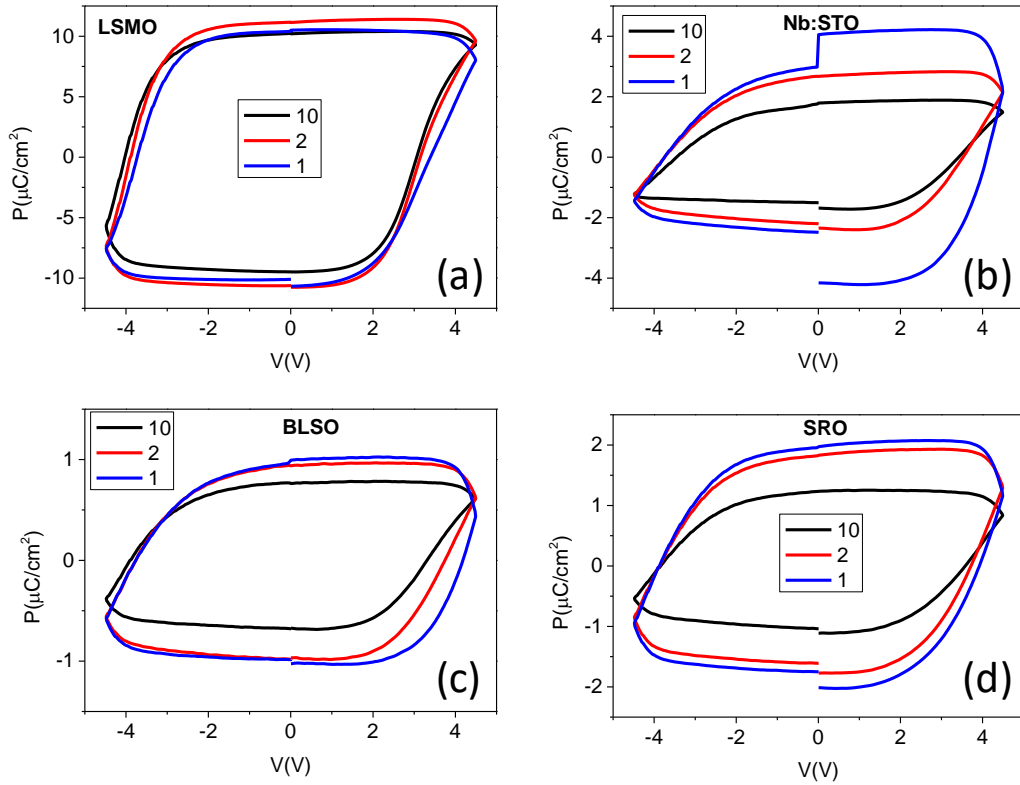


Figure S3. P-V curves of the HZO films on (a) LSMO, (b) Nb:STO, (c) BLSO and (d) SRO. Each panel shows polarization loop for the first, second and tenth cycle collected in a pristine junction of the sample.

#### S4 $\theta$ - $2\theta$ scans of HZO films on BLSO, SRO, Nb:STO, LSMO and LNO electrodes

Figure S4 shows the  $\theta$ - $2\theta$  scans measured with point detector ( $\chi=0^\circ$ ) of the HZO films on LNO, LSMO, SRO, BLSO and Nb:STO electrodes. In accordance with the results shown in Figure 1, the o-HZO(111) reflection at  $\chi=0^\circ$  is only observed in the film grown on LSMO. Due to the big dispersion in  $\chi$  around  $\chi=0^\circ$  (see Figure 1), the m-HZO(002) reflection is almost not observable in the films grown on LSMO and LNO, and not observable in the film on SRO (Figure S4 (b)).

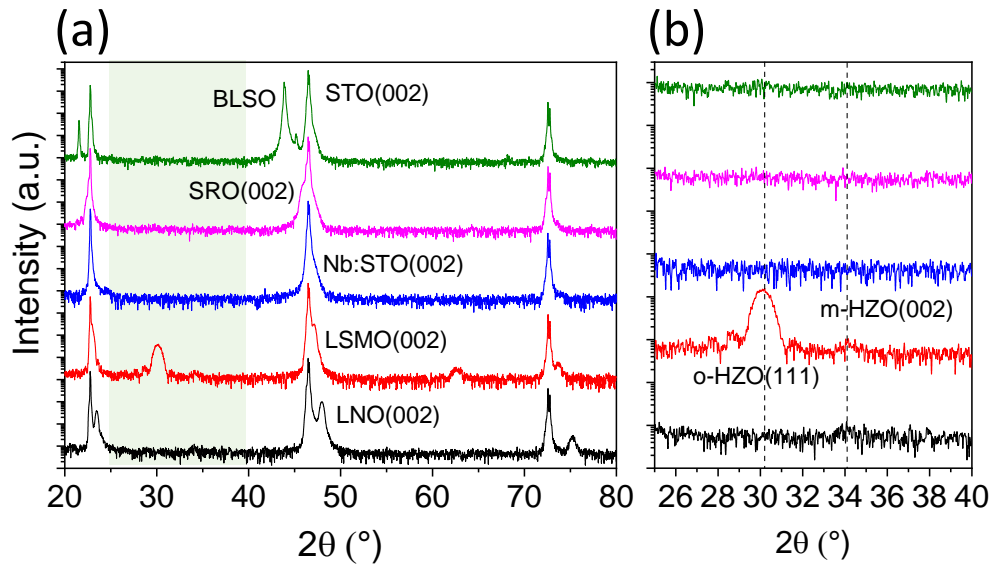


Figure S4. (a) XRD  $\theta$ - $2\theta$  scans of the HZO films on LNO, LSMO, SRO, BLSO and Nb:STO electrodes measured with point detector ( $\chi=0$ ). (b) shows the  $\theta$ - $2\theta$  scans zoomed in the range  $2\theta=25$ - $40^\circ$ .

#### S5 $\theta$ - $2\theta$ scans of the HZO films on LSMO/SRO, LSMO/LNO, SRO/LSMO and LNO/LSMO bilayer electrodes

Figure S5 shows the  $\theta$ - $2\theta$  scans measured with point detector ( $\chi=0^\circ$ ) of the HZO films on LSMO/SRO, LSMO/LNO, SRO/LSMO and LNO/LSMO bilayer electrodes. In accordance with the results shown in Figure 5, the o-HZO(111) reflection at  $\chi=0$  is observed in the films grown on LSMO/SRO, LSMO/LNO and with a smaller peak on SRO/LSMO (Figure S5 (b)). The m-HZO(002) reflection is barely visible in the said films, while it is visible in the film grown on LNO/LSMO. The bigger intensity of the m-HZO(002) on LNO/LSMO than on SRO/LSMO is mainly due to its smaller mosaicity along  $\chi$  (see Figure 3, notice the logarithmic scale used).

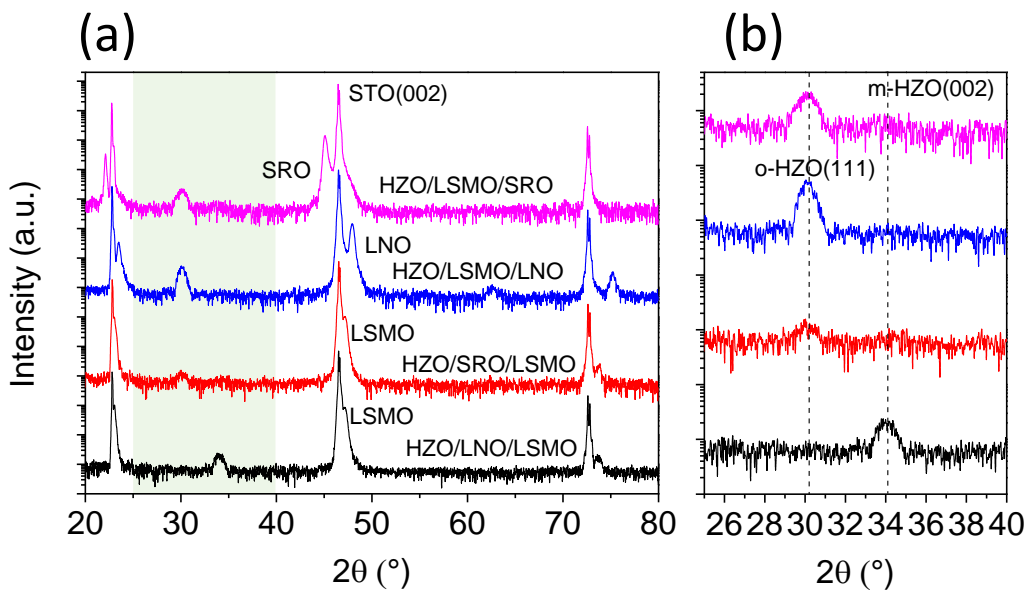


Figure S5. (a) XRD  $\theta$ - $2\theta$  scans of the HZO films on LSMO/SRO, LSMO/LNO, SRO/LSMO and LNO/LSMO bilayer electrodes measured with point detector ( $\chi=0$ ). (b) shows the  $\theta$ - $2\theta$  scans zoomed in the range  $2\theta=25$ - $40^\circ$ .

### S6 Scanning transmission electron microscopy images

Scanning transmission electron microscopy was used to study the samples with high spatial resolution in real space. For this aim, a JEOL AMR200cF microscope equipped with a spherical aberration corrector, operated at 200 kV, was used. Figures S6 (a) and (b) show high field of view cross-sectional Z-contrast images of the HZO films on bilayer electrodes with ultra-thin SRO and LNO layers in contact with the HZO, respectively. As can be appreciated in the corresponding high magnification images presented in Figure S6 (c) and (d), SRO tends to accumulate in 3-D grains leaving areas of the LSMO surface uncovered, suggesting an island-like growth mode of the top layer. On the other hand, LNO forms a thin continuous layer of homogeneous thickness that fully covers the LSMO surface. Note that the LNO layer can be easily identified due to the higher intensity of the atomic columns of LNO compared to those of the LSMO layer (Figure S6 (d)). This difference arises from the larger La content (which is a heavier element  $Z_{La}=57$ ,  $Z_{Sr}=38$ ) of the LNO layer. While the high resolution Z-contrast images of the inspected areas revealed monoclinic grains with both (100) and (001) out-of-plane orientations in both samples, XRD (Figure S4 and Figure 3) shows that (001) is the dominant orientation.

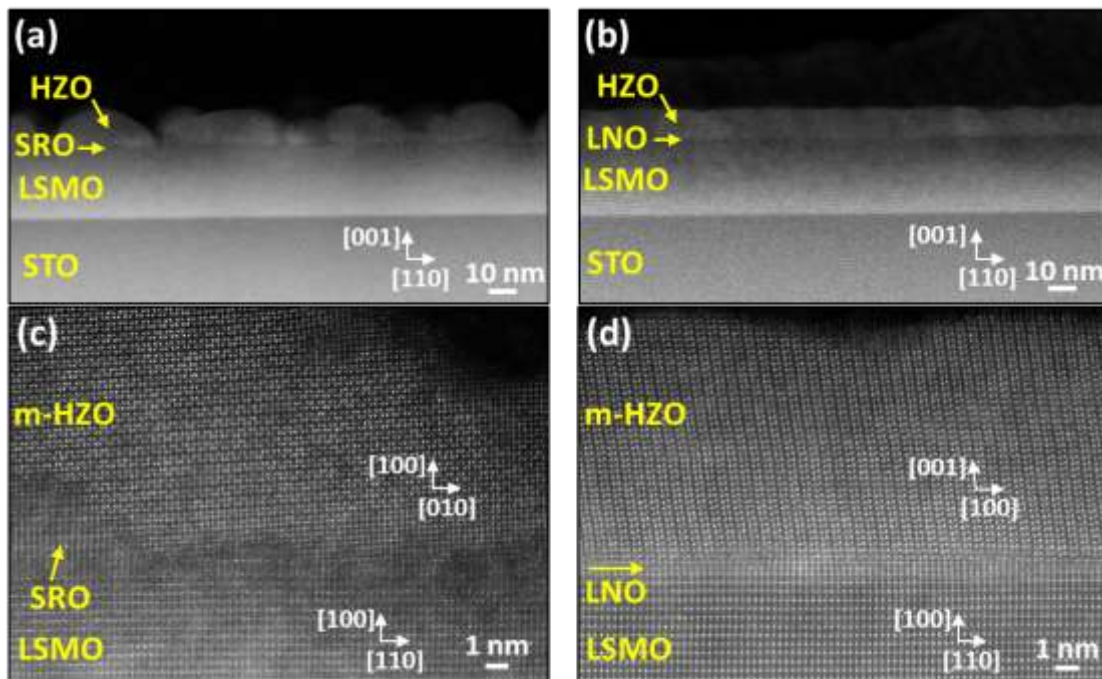


Figure S6. (a) and (b) show high field of view cross-sectional Z-contrast images of the HZO films on bilayer electrodes with ultra-thin SRO and LNO layers in contact with the HZO, respectively. (c) and (d) exhibit the atomic resolution images corresponding to the LSMO electrode, the SRO (c) and LNO (d) ultra-thin layers, and the HZO film.

### S7 $\theta$ - $2\theta$ scans of the HZO films on $\text{La}_{1-x}\text{A}_x\text{MnO}_3$ ( $\text{A} = \text{Sr, Ca}; x = 0.33, 0.5$ ) electrodes

Figure S7 shows the  $\theta$ - $2\theta$  scans measured with point detector ( $\chi=0^\circ$ ) of the HZO films on  $\text{La}_{1-x}\text{A}_x\text{MnO}_3$  ( $\text{A} = \text{Sr, Ca}; x = 0.33, 0.5$ ) electrodes. In accordance with the results shown in Figure 4, the o-HZO(111) reflection at  $\chi=0$  is bigger in the samples grown on  $\text{La}_{0.67}\text{Sr}_{0.33}\text{MnO}_3$  and  $\text{La}_{0.67}\text{Ca}_{0.33}\text{MnO}_3$ , and smaller on those grown on  $\text{La}_{0.5}\text{Sr}_{0.5}\text{MnO}_3$  and  $\text{La}_{0.5}\text{Ca}_{0.5}\text{MnO}_3$ .

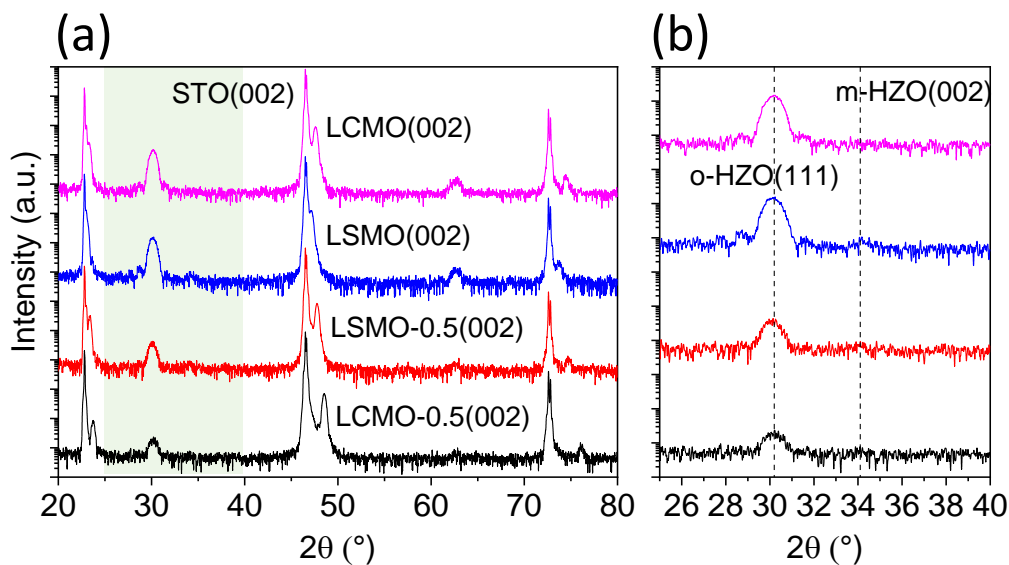


Figure S7. (a) XRD  $\theta$ - $2\theta$  scans of the HZO films on  $\text{La}_{1-x}\text{A}_x\text{MnO}_3$  ( $\text{A} = \text{Sr, Ca}; x = 0.33, 0.5$ ) electrodes measured with point detector ( $\chi=0$ ). (b) shows the  $\theta$ - $2\theta$  scans zoomed in the range  $2\theta=25$ - $40^\circ$ .

## S8 P-E loops collected during the first 10 cycles for HZO films on BLSO, SRO, Nb:STO, LSMO electrodes

In Figure S8(a,b,c,d), representative loops collected during the first 10 cycles in films grown on LSMO, LCMO, LSMO-0.5 and LCMO-0.5, respectively, are shown. It is observed that for films grown on LCMO, LSMO-0.5 and LCMO-0.5, the change in the P-E shape and extracted  $P_r$  value is not as large as for the films grown on Nb:STO and BLSO but more noticeable than for the film grown on LSMO.

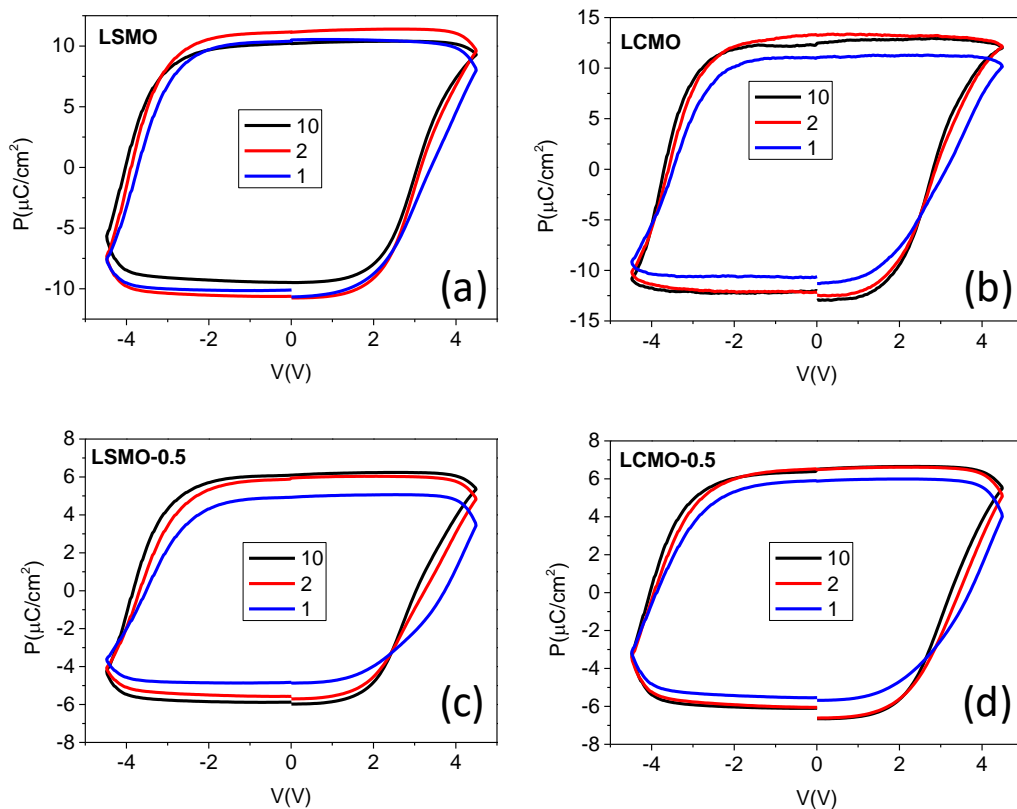


Figure S8. P-V curves of the HZO films on (a) LSMO, (b) LCMO, (c) LSMO-0.5 and (d) LCMO-0.5. Each panel shows polarization loop for the first, second and tenth cycle collected in a pristine junction of the sample.

## References

- 1 T. Song, R. Bachelet, G. Saint-Girons, R. Solanas, I. Fina, F. Sánchez, *ACS Appl. Electron. Mater.* 2020, **2**, 3221.